

# Transverse momentum diffusion and jet energy loss in non-Abelian plasmas

Björn Schenke,<sup>1, 2</sup> Michael Strickland,<sup>2, 3</sup>  
 Adrian Dumitru,<sup>4, 5</sup> Yasushi Nara,<sup>6</sup> and Carsten Greiner<sup>2</sup>

<sup>1</sup>*Department of Physics, McGill University,  
 H3A 2T8, Montreal, Quebec, Canada*

<sup>2</sup>*Institut für Theoretische Physik, Goethe - Universität Frankfurt  
 Max-von-Laue-Straße 1, D-60438 Frankfurt am Main, Germany*

<sup>3</sup>*Gettysburg College, Gettysburg, PA 17325, USA*

<sup>4</sup>*Department of Natural Sciences, Baruch College, CUNY,  
 17 Lexington Avenue, New York, NY 10010, USA*

<sup>5</sup>*RIKEN BNL Research Center, Brookhaven National Laboratory, Upton, NY 11973, USA*

<sup>6</sup>*Akita International University 193-2 Okutsukakidai,  
 Yuwa-Tsubakigawa, Akita-City, Akita 010-1211, Japan*

## Abstract

We consider momentum broadening and energy loss of high momentum partons in a hot non-Abelian plasma due to collisions and soft gluon radiation. We solve the coupled system of Wong-Yang-Mills equations on a lattice in real time, including binary hard elastic collisions among the partons. The collision kernel is constructed such that the total collisional energy loss and momentum broadening are lattice spacing independent. We find that the transport coefficient  $\hat{q}$  receives sizeable contributions from a power-law tail in the  $p_\perp$ -distribution of high-momentum partons. Also, that induced radiation of soft gluons above the thermal wavelength dominates  $dE/dx$  by an order of magnitude as compared to elastic collisions at very high temperature,  $T \gtrsim 1 - 2$  GeV.

PACS numbers: 11.15.Kc, 12.38.Mh, 24.10.Lx, 24.85.+p, 25.75.Bh

## I. INTRODUCTION

The study of high transverse momentum jets produced in heavy-ion collisions can provide information on the properties of the hot QCD plasma produced in the central rapidity region [1, 2, 3, 4, 5, 6, 7, 8, 9, 10, 11, 12, 13, 14, 15, 16, 17, 18, 19, 20]. After the discovery of jet quenching at the Relativistic Heavy Ion Collider (RHIC) [2, 3] a lot of progress has been made towards using jets as a quantitative tomographic probe of the QGP. Jet quenching refers to the suppression of high transverse momentum hadrons, such as  $\pi^0$  and  $\eta$  mesons in central  $Au + Au$  collisions compared to expectations from measurements in  $p + p$  collisions. Whereas pions and  $\eta$ -mesons exhibit the same suppression at high  $p_\perp$ , direct photons were found to be unsuppressed [21]. This indicates that the observed suppression is related to the absorption (energy loss) of energetic partons in the medium. A quantitative measure of jet quenching is the nuclear modification factor  $R_{AA}$ , the measured yield of hadrons relative to the expected yield from proton-proton reactions scaled by the ratio of the incident parton flux of two gold nuclei to that of two protons. In contrast to direct photons, high- $p_\perp$  mesons are suppressed by a factor of 5 ( $R_{AA} \simeq 0.2$ ).

Additional evidence for the color opacity of the medium is obtained from studies of the angular correlation of the radiation associated with a high- $p_\perp$  trigger particle [22, 23]. In  $p + p$  and  $d + Au$  collisions, a hard recoiling hadron occurs at 180 degrees in azimuth relative to the trigger, reflecting the back-to-back nature of jets at leading-order in QCD. In contrast, central  $Au + Au$  collisions show a strong suppression of such recoils, accompanied by an enhancement and broadening of low- $p_\perp$  particle production. Detailed analyses indicate that the response of the medium to the passage of an energetic parton may be of a characteristic hydrodynamical nature: the energy lost by a high-energy parton may re-appear as a collective Mach cone [24, 25, 26, 27, 28, 29]. Furthermore, recent measurements of di-hadron correlations provide evidence for an asymmetric broadening of jet profiles in the plane of pseudo-rapidity ( $\eta$ ) and azimuthal angle ( $\phi$ ). The interaction with the medium causes a much stronger broadening in  $\eta$  than in  $\phi$  [30, 31, 32, 33, 34], the so-called “ridge”. The detailed origin of this effect is yet unknown, while many theoretical models suggest explanations of different kinds [35, 36, 37, 38, 39, 40, 41, 42, 43, 44, 45, 46].

To learn about the coupling of hard partons to the plasma, in this work we study the dynamic energy loss and momentum broadening of massless high momentum partons traversing

a non-Abelian  $SU(2)$  plasma. Soft multi-particle interactions are treated by solving the coupled system of Wong-Yang-Mills equations in real time. In addition, particles can undergo hard elastic collisions. The main purpose of this paper is to extract lattice-spacing independent results for the transport coefficient  $\hat{q}$  associated with broadening of the momentum distribution of gluon jets, as well as for collisional energy loss  $dE/dx$ . Previous publications [41, 42] already presented a calculation of  $\hat{q}$  within this approach, however lacking the detailed analysis we present here, where we also include the computation of the energy loss  $dE/dx$ . Furthermore, in this paper we extract the entire  $p_\perp^2$  distribution of jets passing through a thermal plasma and not only its first moment  $\hat{q}$ .

So far, estimates based on perturbative QCD (pQCD) of the strength of the coupling of jets to a plasma are sensitive to infrared cutoffs. Also, they are often restricted to systems that are (at least locally) in thermal equilibrium. The problem does not arise in the Wong-Yang-Mills simulation [47, 48, 49, 50, 51, 52, 53, 54, 55, 56], since the soft sector is described by classical chromo-fields. It is separated from the hard sector corresponding to hard elastic pQCD processes. The soft sector is non-perturbative but in an essentially classical way because the occupation number of field modes below the saturation momentum (or temperature) are large [57, 58].

Treating the regimes of hard and soft momentum exchange separately, we obtain results for the *collisional* energy loss  $dE/dx|_{\text{coll}}$  and for the transport coefficient  $\hat{q}|_{\text{coll}}$  which are independent of the exact scale separating the two regimes. We shall find that the total collisional and radiative energy loss, which so far includes soft bremsstrahlung but no hard particle splitting or recombination, satisfies  $dE/dx|_{\text{rad}} \gg dE/dx|_{\text{coll}}$  at very high temperatures. On the other hand,  $\hat{q}|_{\text{tot}} \gtrsim \hat{q}|_{\text{coll}}$ .

We present the temperature, density and jet energy dependence of both  $\hat{q}$  and  $dE/dx$ . Our results are in qualitative agreement with pQCD expectations. We extract a value for  $\hat{q}|_{\text{coll}}$  of  $3.6 \pm 0.3 \text{ GeV}^2 \text{ fm}^{-1}$  at  $T = 400 \text{ MeV}$  in a thermal  $SU(3)$  background for a parton with energy  $E = 19.2 \text{ GeV}$ . This value is in line with results from various other calculations (see [59]). For the energy loss we obtain  $dE/dx|_{\text{coll}} = 1.6 \pm 0.4 \text{ GeV fm}^{-1}$ . Comparing  $dE/dx$  for colored versus colorless jets we are able to isolate the effect of soft bremsstrahlung on top of elastic collisions. We find that at very high temperature the radiation of soft gluons increases  $dE/dx$  by about an order of magnitude.

This paper is organized as follows: We introduce the Boltzmann-Vlasov equations as

well as the Wong equations for non-Abelian plasmas in Sec. II, and discuss the lattice implementation in Sec. III. We outline how collisions are included into the Wong-Yang-Mills simulation in Sec. IV, and describe how the separation between the soft and hard sector is done in Sec. V. After discussing the initialization of the simulation in Sec. VI, we present results for collisional energy loss and for momentum broadening in Sec. VII A, and for radiative energy loss in Sec. VII B. Finally, we close with conclusions in Sec. VIII.

## II. BOLTZMANN-VLASOV EQUATION FOR NON-ABELIAN GAUGE THEORIES

The classical transport theory for non-Abelian plasmas has been established by Heinz and Elze [60, 61, 62, 63]. Here, we solve numerically the classical transport equation for hard gluons with adjoint  $SU(2)$  color charge  $q = q^a \tau^a$ , where the  $\tau^a$  are the color generators, including hard binary collisions

$$p^\mu (\partial_\mu + g q^a F_{\mu\nu}^a \partial_p^\nu + g f^{abc} A_\mu^b(x) q^c \partial_{q^a}) f = \mathcal{C}. \quad (1)$$

$f = f(x, p, q)$  denotes the single-particle phase space distribution,  $F_{\mu\nu}^a = \partial_\mu A_\nu^a - \partial_\nu A_\mu^a - g f^{abc} A_\mu^b A_\nu^c$  is the gauge field strength tensor,  $g$  the gauge coupling,  $A_\mu^a$  the soft gauge field, and  $\mathcal{C}$  is the collision term to be defined below. It is coupled self-consistently to the Yang-Mills equation for the soft gluon fields,

$$D_\mu F^{\mu\nu} = j^\nu = g \int \frac{d^3 p}{(2\pi)^3} dq q v^\nu f(x, p, q), \quad (2)$$

with  $v^\mu = (1, \mathbf{p}/p)$ . For  $\mathcal{C} = 0$  these equations reproduce the “hard thermal loop” effective action near equilibrium [64, 65, 66]. However, the full classical transport theory (1,2) also includes some higher  $n$ -point vertices of the dimensionally reduced effective action for static gluons [67] beyond the hard-loop approximation. The back-reaction of the long-wavelength fields on the hard particles (“bending” of their trajectories) is taken into account. This is essential for achieving cutoff independent results for the transport coefficient  $\hat{q}$  and for the energy loss  $dE/dx$  of high momentum partons.

When the phase-space density is parametrically small,  $f = \mathcal{O}(1)$ , which is the case for hard momenta, the collision term is given by

$$\mathcal{C} = \frac{1}{4E_1} \int_{\mathbf{p}_2} \int_{\mathbf{p}'_1} \int_{\mathbf{p}'_2} (2\pi)^4 \delta^{(4)}(p'_1 + p'_2 - p_1 - p_2) (f'_1 f'_2 |\mathcal{M}_{1'2' \rightarrow 12}|^2 - f_1 f_2 |\mathcal{M}_{12 \rightarrow 1'2'}|^2), \quad (3)$$

with  $\int_{\mathbf{p}_i} = \int \frac{d^3 p_i}{(2\pi)^3 2E_i}$ . The matrix element  $\mathcal{M}$  includes all  $gg \rightarrow gg$  tree-level diagrams shown in Fig. 1, and color factors as appropriate for the  $SU(2)$  gauge group.

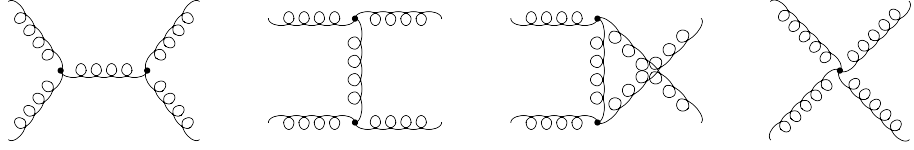


FIG. 1: Processes contributing to  $gg \rightarrow gg$  scattering at leading order.

We employ the test particle method and replace the continuous distribution  $f(x, p, q)$  by a large number of test particles [68]:

$$f(\mathbf{x}, \mathbf{p}, q) = \frac{1}{N_{\text{test}}} \sum_i \delta^3(\mathbf{x} - \mathbf{x}_i(t)) (2\pi)^3 \delta^{(3)}(\mathbf{p} - \mathbf{p}_i(t)) \delta^{(N^2-1)}(q - q_i(t)), \quad (4)$$

which leads to the Wong equations [47] (also see [69, 70])

$$\dot{\mathbf{x}}_i(t) = \mathbf{v}_i(t), \quad (5)$$

$$\dot{\mathbf{p}}_i(t) = gq_i^a(t) (\mathbf{E}^a(t) + \mathbf{v}_i(t) \times \mathbf{B}^a(t)), \quad (6)$$

$$\dot{q}_i(t) = -igv_i^\mu(t) [A_\mu(t), q_i(t)]. \quad (7)$$

Here,  $\mathbf{x}_i(t)$ ,  $\mathbf{v}_i(t)$ , and  $q_i(t)$ , are the position, velocity<sup>1</sup> and color charge of the  $i^{\text{th}}$  test particle.  $N_{\text{test}}$  denotes the number of test particles per physical particle,  $A_\mu(t) = A_\mu^a(t)\tau^a$  and the commutator commutes color generators  $\tau^a$ . The last equation (7) describes the precession of the color charge  $q_i(t)$  due to the color fields.

Writing the current in terms of the individual test particles, the Yang-Mills equation for the soft gluon fields becomes

$$D_\mu F^{\mu\nu} = J^\nu = \frac{g}{N_{\text{test}}} \sum_i q_i v_i^\nu \delta(\mathbf{x} - \mathbf{x}_i(t)). \quad (8)$$

The theory without collisions as given by equations (5-7) coupled to the lattice Yang-Mills equations (8) was first solved in [71] to study Chern-Simons number diffusion in non-Abelian gauge theories at finite temperature. It was applied later also to the problem of gauge-field instabilities in anisotropic  $SU(2)$  plasmas [55, 56]. Our numerical implementation is based

<sup>1</sup> We consider only massless particles here so that  $|\mathbf{v}_i| = 1$ .

on the improved formulation detailed in [56] where the non-Abelian currents, generated by the hard particle modes on the lattice sites, are “smeared” in time (the charges are smeared in space). This technique makes simulations in three dimensions on large lattices possible in practice.

### III. REAL-TIME LATTICE SIMULATION

The time evolution of the Yang-Mills field is determined by the standard Hamiltonian method in  $A^0 = 0$  gauge [48, 71, 72]. The temporal gauge is particularly useful because it allows for a simple identification of the canonical momentum as the electric field

$$\mathbf{E}^a = -\dot{\mathbf{A}}^a. \quad (9)$$

In addition, time-like link variables  $U$ , defined below, become simple identity matrices.

The lattice Hamiltonian in this gauge is given by [73]

$$H_L = \frac{1}{2} \sum_i \mathbf{E}_L^a \cdot \mathbf{E}_L^a + \frac{1}{2} \sum_{\square} (N_c - \text{ReTr}U_{\square}) + \frac{1}{N_{\text{test},L}} \sum_j |\mathbf{p}_{Lj}|, \quad (10)$$

including the particle contribution  $1/N_{\text{test},L} \sum_j |\mathbf{p}_{Lj}|$ . The plaquette is defined by

$$U_{\square} = U_x(i)U_y(i + \hat{x})U_x^{\dagger}(i + \hat{y})U_y^{\dagger}(i), \quad (11)$$

with the link variable

$$U_{\mu}(i) = e^{iagA_{\mu}(i)}. \quad (12)$$

Note that the index  $\mu$  on  $U$  is merely an indicator of its direction and not a Lorentz index. The shifts  $\hat{x}$  and  $\hat{y}$  are one lattice spacing in length and directed into the  $x$ - or  $y$ - direction, respectively.<sup>2</sup>

Eq. (10) is given in lattice units, which are chosen such that all lattice variables are dimensionless:

$$\mathbf{E}_L^a = \frac{ga^2}{2}\mathbf{E}^a, \quad \mathbf{B}_L^a = \frac{ga^2}{2}\mathbf{B}^a, \quad \mathbf{p}_L = \frac{a}{4}\mathbf{p}, \quad Q_L^a = \frac{1}{2}q^a, \quad N_{\text{test},L} = \frac{1}{g^2}N_{\text{test}}, \quad (13)$$

---

<sup>2</sup> We set  $\tau_a = \sigma_a$ , the Pauli matrices, without the usual factor of  $1/2$ , i.e., the commutation relation reads  $[\tau^a, \tau^b] = 2\delta^{ab}$ . Another factor of  $1/2$  is absorbed into the  $A$ -field, which has to be taken into account when calculating the physical fields  $\mathbf{E}$  and  $\mathbf{B}$  from it.

with the lattice spacing  $a$ .  $H_L$  is hence related to the physical Hamiltonian by  $H = 4/(g^2 a) H_L$ . To convert lattice variables to physical units we will fix the lattice length  $L$  in fm, which will then determine the physical scale for  $a$ . All other dimensionful quantities can then be determined from Eqs. (13). The Hamiltonian (10) determines the energy density of the system and enters the equations of motion for the fields, e.g.,

$$\frac{d}{dt} \mathbf{E}_L = \{\mathbf{E}_L, H_L\} , \quad (14)$$

with the Poisson bracket  $\{\cdot, \cdot\}$ . Our lattice has periodic boundary conditions in all spatial directions.

#### IV. COLLISIONS

The collision kernel (3) is similar to that used in (parton) cascade simulations [74, 75, 76, 77, 78, 79, 80, 81, 82, 83]. However, there is no need to suppress momentum exchanges below the Debye-mass ( $\sim gT$ ). Soft multi-parton interactions are mediated by interactions with the collective Yang-Mills field. This way, we are able also to study collective phenomena and their contribution to isotropization and thermalization. In particular, we can in principle also study systems far from equilibrium (see [41]) for which the scale corresponding to the Debye-mass squared in an isotropic system becomes negative [84, 85, 86, 87]. In this case it can obviously not damp the propagator to act as a cut off for the momentum exchange in the infrared.

To complete our dual particle/field description, we need to specify the separation scale  $k^*$  between the field and particle degrees of freedom. We will discuss this separation scale in detail below. For now it will serve as a lower bound for the exchanged momenta for binary elastic particle collisions. All softer momentum exchanges are mediated by the fields.

The collision term (3) is incorporated using the stochastic method introduced and applied in [82, 88, 89]. We do not interpret the cross section in a geometrical way as done in [74, 76, 77, 78, 79, 80] but determine scattering processes in a stochastic manner by sampling possible transitions in a volume element per time interval. This collision algorithm can be extended to include inelastic processes  $gg \leftrightarrow ggg$  as done in [82, 83], which will also be incorporated in the future in our simulations.

The collision rate in a spatial volume element  $\Delta^3 x$  per unit phase space for a particle

pair with momenta in the range  $(\mathbf{p}_1, \mathbf{p}_1 + \Delta^3 p_1)$  and  $(\mathbf{p}_2, \mathbf{p}_2 + \Delta^3 p_2)$  follows from Eq. (3)

$$\begin{aligned} \frac{\Delta N_{\text{coll}}}{\Delta t \frac{1}{(2\pi)^3} \Delta^3 x \Delta^3 p_1} &= \frac{1}{2E_1} \frac{\Delta^3 p_2}{(2\pi)^3 2E_2} f_1 f_2 \\ &\times \frac{1}{2} \int \frac{d^3 p_1'}{(2\pi)^3 2E_1'} \frac{d^3 p_2'}{(2\pi)^3 2E_2'} |\mathcal{M}_{12 \rightarrow 1'2'}|^2 (2\pi)^4 \delta^{(4)}(p_1 + p_2 - p_1' - p_2'). \end{aligned} \quad (15)$$

Expressing the distribution functions as

$$f_i = \frac{\Delta N_i}{\frac{1}{(2\pi)^3} \Delta^3 x \Delta^3 p_i}, \quad i = 1, 2, \quad (16)$$

and employing the usual definition of the cross section for massless particles [90]

$$\sigma_{22} = \frac{1}{4s} \int \frac{d^3 p_1'}{(2\pi)^3 2E_1'} \frac{d^3 p_2'}{(2\pi)^3 2E_2'} |\mathcal{M}_{12 \rightarrow 1'2'}|^2 (2\pi)^4 \delta^{(4)}(p_1 + p_2 - p_1' - p_2'), \quad (17)$$

one obtains the total collision probability in a volume element  $\Delta^3 x$  and time interval  $\Delta t$ :

$$P_{22} = \frac{\Delta N_{\text{coll}}}{\Delta N_1 \Delta N_2} = \tilde{v}_{\text{rel}} \sigma_{22} \frac{\Delta t}{\Delta^3 x}. \quad (18)$$

$\tilde{v}_{\text{rel}} = s/2E_1 E_2$  denotes the relative velocity, where  $s$  is the invariant mass of the particle pair.  $P_{22}$  is a number between 0 and 1.<sup>3</sup> Whether or not a collision occurs is sampled stochastically as follows: We compare  $P_{22}$  to a uniformly distributed random number between 0 and 1. If the random number is less than  $P_{22}$ , the collision does occur. Otherwise, there is no collision between the two particles in that time step. Since we represent each physical particle by  $N_{\text{test}}$  test particles, we have to rescale the cross section as  $\sigma \rightarrow \sigma/N_{\text{test}}$ . This leads to

$$P_{22} = \tilde{v}_{\text{rel}} \frac{\sigma_{22}}{N_{\text{test}}} \frac{\Delta t}{\Delta^3 x}. \quad (19)$$

To determine this probability, we require the total cross section  $\sigma_{22}$ . To leading order in  $\alpha_s$  it follows from the differential cross section obtained from the diagrams in Fig. 1 [91, 92, 93]:

$$\frac{d\sigma}{dt} = \frac{4\pi\alpha_s^2}{s^2} \frac{N_c^2}{N_c^2 - 1} \left( 3 - \frac{tu}{s^2} - \frac{su}{t^2} - \frac{st}{u^2} \right), \quad (20)$$

with  $N_c$  the number of colors. In particular, for SU(2) and SU(3), respectively,

$$\frac{d\sigma}{dt} = \frac{16\pi\alpha_s^2}{3s^2} \left( 3 - \frac{tu}{s^2} - \frac{su}{t^2} - \frac{st}{u^2} \right) \quad \text{for SU(2)}, \quad (21)$$

$$\frac{d\sigma}{dt} = \frac{9\pi\alpha_s^2}{2s^2} \left( 3 - \frac{tu}{s^2} - \frac{su}{t^2} - \frac{st}{u^2} \right) \quad \text{for SU(3)}. \quad (22)$$

---

<sup>3</sup> In practice one has to choose suitable  $\Delta^3 x$  and  $\Delta t$  to ensure that  $P_{22} < 1$ .

The invariant Mandelstam variables are

$$s = (P_1 + P_2)^2, \quad t = (P_1 - P'_1)^2, \quad u = (P_1 - P'_2)^2. \quad (23)$$

Using  $t = -q^2$ , with  $q$  the momentum transfer, and the identity  $s + t + u = 0$  for massless particles, we can express the total cross section for processes with  $\sqrt{q^2}$  larger than  $k^*$  as

$$\sigma_{22} = \int_{k^*}^{s/2} \frac{d\sigma}{dq^2} dq^2. \quad (24)$$

The momentum transfer is then determined stochastically in the center-of-momentum frame of the two colliding particles from the probability distribution

$$\mathcal{P}(q^2) = \frac{1}{\sigma_{22}} \frac{d\sigma}{dq^2}. \quad (25)$$

In Eq. (24) we have introduced the cutoff  $k^*$  for point-like binary collisions. To avoid double-counting, this cutoff should be on the order of the hardest field mode that can be represented on the given lattice,  $k^* \simeq \pi/a$ .

## V. SEPARATION SCALE

The scattering processes in the regime of hard momentum exchange are described by elastic binary collisions, while soft momentum exchanges are mediated by the fields. A scattering in the soft regime corresponds to deflection of a particle in the field of the other(s).

Physically, the separation scale  $k^*$  should be sufficiently small so that the soft field modes below  $k^*$  are highly occupied [72] and hence can be described classically. On the other hand,  $k^*$  should be sufficiently large to ensure that hard modes can be represented by particles and that collisions are described by (3), which is valid only for low occupation numbers since the Bose enhancement factor  $(1 + f)$  is approximated by 1. In practice  $g \sim 1$ , and we choose  $k^*$  to be on the order of the temperature. At the same time,  $k^*$  is related to the hardest available field mode, which on a cubic lattice is given by  $\sqrt{3}\pi/a$ . Obviously, any matching between soft and hard regimes can only be done approximately, because the lattice on which the field modes are defined is cubic, while the momentum space cutoff of the hard collision integral is implicitly spherical.

The “soft” scale is given by

$$m_D^2 = g^2 N_c \int \frac{d^3 p}{(2\pi)^3} \frac{f(\mathbf{p})}{|\mathbf{p}|} \sim g^2 N_c \frac{n_g}{p_h}, \quad (26)$$

where  $N_c = 2$  is the number of colors and  $n_g$  denotes the number density of hard gluons, summed over two helicities and  $N_c^2 - 1$  colors. Also,  $p_h \approx 3T$  is the typical momentum of a hard particle from the medium.

To allow for reliable numerical simulations one should have  $m_DL \gg 1$  and  $m_D a \ll 1$ . The first condition ensures that the relevant soft modes actually fit on the lattice while the latter ensures that the lattice can resolve the wavelength  $1/m_D$  to good precision.

As we have argued above, we shall choose the inverse lattice spacing to be on the order of the temperature of the medium. Thus, with (26) the condition  $m_D a \ll 1$  roughly translates to

$$g^2 N_c \frac{n_g}{T^3} \ll 1 . \quad (27)$$

In order to satisfy this relation, which is essentially the weak-coupling condition, at  $g \sim 1$ , we perform our numerical simulations below for an extremely hot and undersaturated medium:  $T^3 \gg n_g$ . This ensures that the simulations are carried out near the continuum limit. We shall verify below that transverse momentum broadening of a high-energy jet passing through a thermal medium is independent of  $T$  if the density and the ratio of jet momentum to temperature is fixed. One may therefore obtain a useful weak-coupling estimate of  $\langle p_\perp^2 \rangle$  (resp. for the related transport coefficient  $\hat{q}$ ) by extrapolating our measurements down to temperatures relevant to present heavy-ion collisions.

## VI. INITIALIZATION

We consider a heat-bath of Boltzmann distributed particles with a density of  $n_g = \{5, 10, 20\} \text{ fm}^{-3}$  and an average particle momentum of  $3T = \{6, 12, 18, 24\} \text{ GeV}$ . For a given lattice (resp.  $k^*$ ) we take the initial energy density of the thermalized fields to be

$$\varepsilon_{\text{fields}} = \int \frac{d^3 k}{(2\pi)^3} k \hat{f}_{\text{Bose}}(k) \Theta(k^* - k) , \quad (28)$$

where

$$\hat{f}_{\text{Bose}}(k) = \frac{n_g}{2T^3 \zeta(3)} \frac{1}{e^{k/T} - 1} \quad (29)$$

is a Bose distribution normalized to the assumed particle density  $n_g$ , and  $\zeta$  is the Riemann zeta function.

The initial field amplitudes are sampled from a Gaussian distribution:  $\langle A_i^a(x) A_j^b(y) \rangle = \frac{4\mu^2}{g^2} \delta_{ij} \delta^{ab} \delta(\mathbf{x} - \mathbf{y})$ . To thermalize the initial fields (approximately), we match their Fourier

spectrum to the classical limit of the Bose distribution. Hence, the initial spectrum is gauge-fixed to Coulomb gauge and a filter is applied such that

$$A_i \sim 1/k$$

(in continuum notation). Setting  $E_i = 0$  initially<sup>4</sup>, Gauss's law implies that the local charge density at time  $t = 0$  vanishes. We ensure that any particular initial condition satisfies exact local charge neutrality. The charge smearing algorithm for SU(2) explicitly exploits (covariant) current conservation and hence Gauss's law is satisfied exactly by construction at all times [56].

The above procedure ensures that there is no large discontinuity of the energy density when going from the field to the particle regime. This way we are able to vary the separation scale  $k^*$  about the temperature  $T$  by varying the lattice spacing. Fig. 2 shows the distribution of field modes and particles and the separation scale  $k^* \sim T$ .

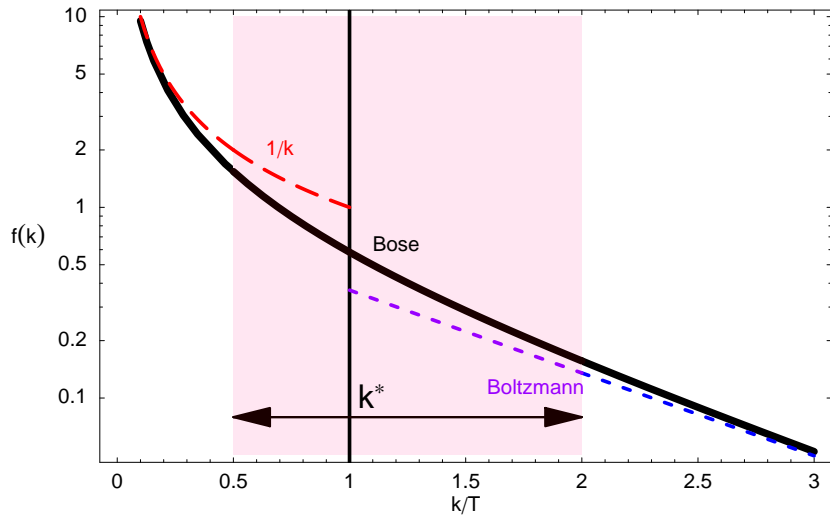


FIG. 2: Bose distribution and its low and high-momentum limits, used for the initial fields and particles, respectively. Physically, the separation  $k^*$  should be on the order of the temperature  $T$ . The band between  $T/2$  and  $2T$  roughly indicates the region within which we shall vary  $k^*$ .

---

<sup>4</sup> Equipartitioning of electric and magnetic fields is achieved very rapidly within a few time steps.

## VII. MOMENTUM DIFFUSION AND ENERGY LOSS OF HIGH MOMENTUM PARTONS

Having initialized the background particles and fields, we can now add a few high-momentum test particles propagating along a given (“longitudinal”) direction which represent the jets. Their density should be sufficiently low so that they do not influence the thermal background significantly and so their mutual interaction is minimized.

We always initialize “bunches” of test particles, which represent one physical hard momentum parton (“jet”). A bunch corresponds to  $N_{\text{test}}$  particles in the same lattice cell. The physical color charge is independent of  $N_{\text{test}}$ . If, in fact, the color charges of all test particles representing one jet add to zero, no coherent radiation is emitted (colorless jet). Such jets can only suffer collisional energy loss<sup>5</sup>. Conversely, to allow for soft radiation, we can initialize a bunch of test particles with aligned color vectors, leading to a net current on the lattice. We do not expect to obtain a lattice-spacing independent result in this case as our collision kernel does not include bremsstrahlung processes (see [81] for an implementation of such processes). Nevertheless, this “colored jet” setup allows us to asses whether soft bremsstrahlung up to momentum  $k^* \sim T$  contributes significantly to jet energy loss.

### A. Collisional energy loss

As detailed above, colorless bunches of test particles permit us to restrict to collisional energy loss and momentum broadening due to elastic collisions only. We first demonstrate that in our approach both

$$\hat{q} = \frac{1}{\lambda\sigma} \int d^2 p_\perp p_\perp^2 \frac{d\sigma}{dp_\perp^2}, \quad (30)$$

and the differential energy loss  $dE/dx$  are independent of the separation scale  $k^*$ . Here and in what follows,  $p_\perp$  denotes the momentum transverse to the initial jet momentum.  $\hat{q}$  can be extracted from the accumulated  $\langle p_\perp^2 \rangle(t) = \langle p_x^2 + p_y^2 \rangle(t)$ . Since  $(1/\sigma)d\sigma/dp_\perp^2$  is the probability distribution for a collision with momentum transfer  $p_\perp$  to occur, the integral in (30) is just  $\sigma \langle p_\perp^2 \rangle_{(1 \text{ collision})}$ . Hence,  $\hat{q} = (1/\lambda) \langle p_\perp^2 \rangle_{(1 \text{ collision})}$ , and dividing the accumulated  $\langle p_\perp^2 \rangle$  by the

---

<sup>5</sup> Note that individual test particles from the bunch are of course *colored* and hence they collide not only with hard thermal particles but also with the modes of the thermal fields.

number of collisions that have occurred up to time  $t$ , which is  $t/\lambda$ , we find

$$\hat{q} = \frac{\langle p_\perp^2 \rangle(t)}{t}. \quad (31)$$

Fig. 3 depicts the contributions to  $\hat{q}$  due to soft and hard collisions, respectively, as well as the total. In these simulations the gluon density of the medium was taken to be  $n_g = 5 \text{ fm}^{-3}$ , the temperature  $T = 4 \text{ GeV}$ , and the jet energy is 16 times the average thermal momentum ( $48T$ ).  $\hat{q}$  is shown as a function of the separation scale  $k^* \sim \sqrt{3\pi/a}$ .

The curves for the total and the soft contributions were averaged over  $\sim 80$  runs for each point. The curve corresponding to the hard sector was obtained by subtracting the result without hard collisions (soft sector only) from the total. The error bars indicate one standard deviation about the mean.

We find that the total value is constant to a good approximation although the contribution due to soft scatterings changes considerably. Below  $k^* \approx T$ , the soft sector contributes less than 10%, while it starts dominating around  $k^* \approx 3T$ . It is evident, therefore, that transport coefficients obtained in the leading logarithmic (LL) approximation from the pure Boltzmann approach (without soft fields) are rather sensitive to the infrared cutoff  $k^*$ , unless the energy  $\sqrt{s}$  is extremely high. In LL approximation,

$$\hat{q} = n_g \left( \frac{4\pi\alpha_s^2 N_c^2}{N_c^2 - 1} \right) \log \left( C^2 \frac{Q^2}{k^{*2}} \right), \quad (32)$$

where  $Q^2 \simeq s$  is the upper bound for the momentum transfer and  $C$  is a constant.

Fig. 4 repeats the same analysis for the energy loss per unit path length,  $dE/dx$ . Again we find a constant total energy loss, and a similar dependence on  $k^*$  of the partial contribution due to soft interactions as for  $\hat{q}$ . We have also verified the  $k^*$ -independence for different temperatures, densities and jet energies. Thus, the above-mentioned matching of soft and hard processes provides estimates for  $\hat{q}$  and  $dE/dx$  which are independent of the artificial separation scale  $k^*$  (and of the lattice spacing  $a$ ). It cures the infrared divergence of the perturbative hard-scattering cross section and does not rely on infrared cutoffs from equilibrium physics such as the Debye mass; thus, calculations are not restricted to equilibrium. On the other hand, the matching procedure might have to be modified for other observables which are sensitive to very different scales. This should be analyzed in the future.

Next, we turn to the density and temperature dependence of  $\hat{q}$  and  $dE/dx$ . Figs. 5 and 6 show the linear rise of  $\hat{q}$  and  $dE/dx$  with the density, which is expected from Eq. (30) and

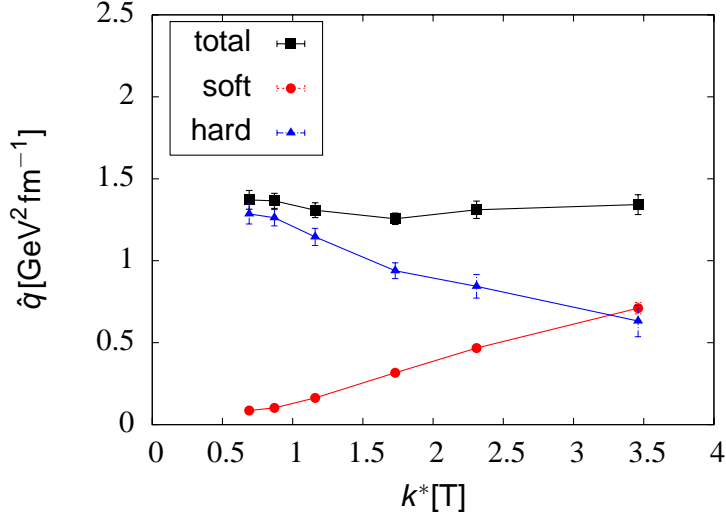


FIG. 3: (In-)dependence of the transport coefficient  $\hat{q}$  on the separation scale  $k^*$ .  $T = 4$  GeV,  $g = 2$ ,  $n_g = 5 \text{ fm}^{-3}$ .

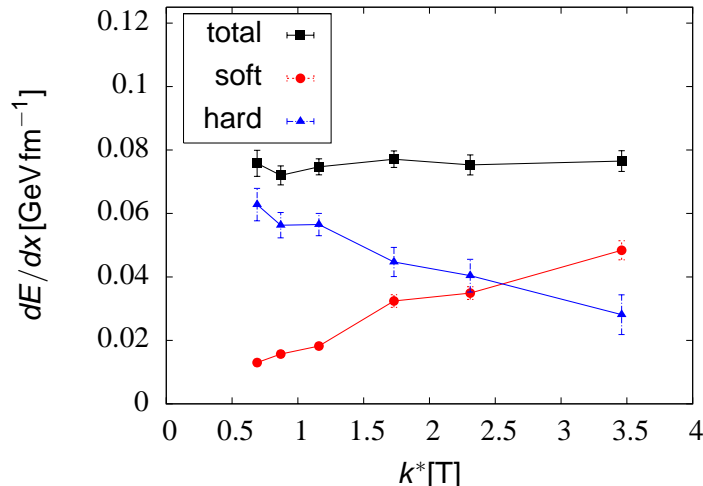


FIG. 4: (In-)dependence of the energy loss  $dE/dx$  on the separation scale  $k^*$ .  $T = 4$  GeV,  $g = 2$ ,  $n_g = 5 \text{ fm}^{-3}$ .

the perturbative results (32) and (33) below, respectively. We will use this linear dependence to extrapolate to slightly larger densities (e.g.,  $n_g^{\text{thermal}}(T = 500 \text{ MeV}) \approx 32 \text{ fm}^{-3}$  for pure glue in SU(3)).

Fig. 7 shows that  $\hat{q}$  is approximately independent of  $T$  as long as the ratio of the jet

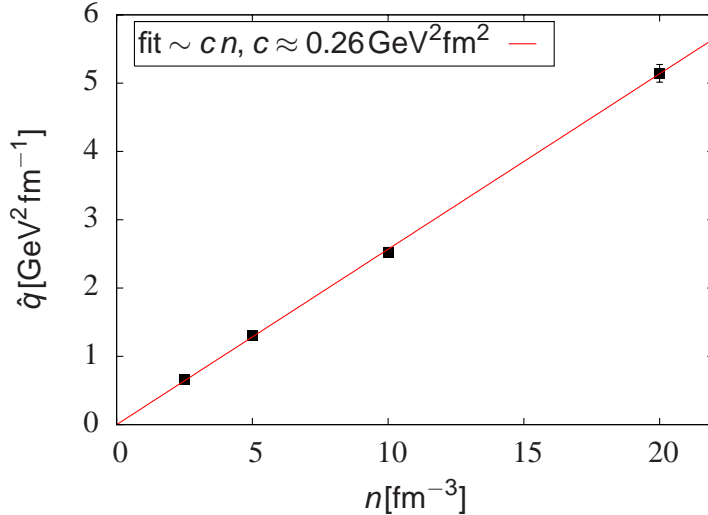


FIG. 5: Linear dependence of  $\hat{q}$  on the density  $n$ .  $T = 4$  GeV,  $g = 2$ ,  $E/T = 48$ ,  $k^* \approx 1.16 T$ . The line shows the best linear fit.

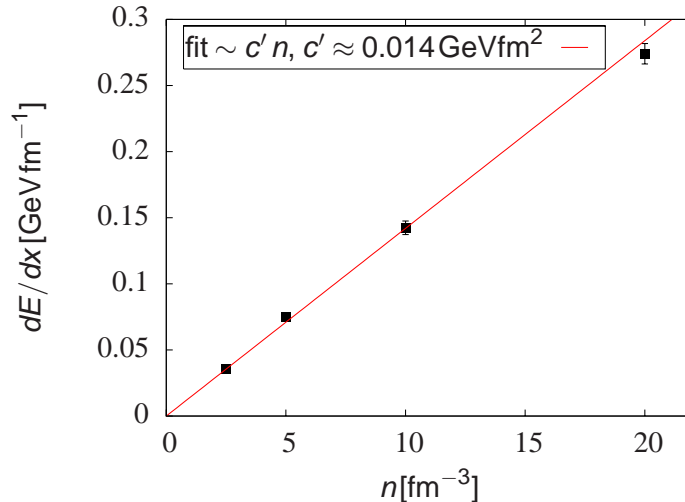


FIG. 6: Linear dependence of  $dE/dx$  on the density  $n$ .  $T = 4$  GeV,  $g = 2$ ,  $E/T = 48$ ,  $k^* \approx 1.16 T$ . The line shows the best linear fit.

energy to the temperature  $E/T$  as well as the density  $n_g$  are fixed. From (32) we expect at most a logarithmic dependence on  $T$ , because  $Q^2 \simeq s$  and  $\langle s \rangle = 6ET$ . The simulation shows that this dependence is very weak.

Fig. 8 shows  $dE/dx$  dropping approximately like  $\sim 1/T$ . This behavior is expected from

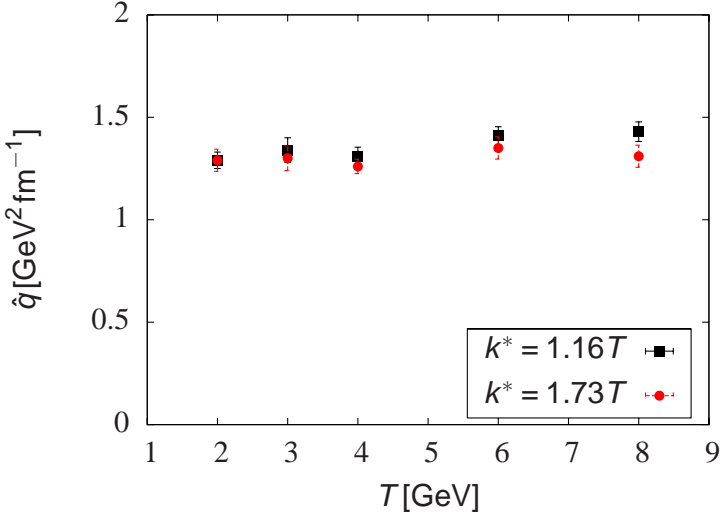


FIG. 7: (In-)dependence of  $\hat{q}$  on the temperature  $T$ .  $n = 5 \text{ fm}^{-3}$ ,  $g = 2$ ,  $E/T = 48$ ,  $k^* \approx 1.16T$  (squares) and  $k^* \approx 1.73T$  (circles).

the perturbative LL result for elastic energy loss (see, for example, ref. [94])

$$\frac{dE}{dx} = n_g \left( \frac{16 \pi \alpha_s^2 N_c^2}{N_c^2 - 1} \right) \frac{E}{s} \log \left( C'^2 \frac{Q^2}{k^*{}^2} \right), \quad (33)$$

where  $s$  is the center-of-mass energy for a process involving scattering of the jet from a hard thermal excitation,  $Q^2 \simeq s$  is the upper limit for the momentum transfer, and  $C'$  is a constant. Because  $\langle s \rangle = 6ET$  this leads to  $dE/dx \sim 1/T$ . Additionally,  $T$  also appears in the logarithm, but this dependence turns out to be weak.

We can now extrapolate to temperatures which are accessible in practice, for which direct computations can not be performed due to the numerical reasons explained above. For an ideal gas of thermal gluons at a temperature  $T$  the density  $n_g = 16T^3\zeta(3)/\pi^2$  (for  $N_c = 3$ ). Using the linear dependence of  $\hat{q}$  on  $n_g$  confirmed above, and its independence on  $T$  for fixed  $n_g$  and  $E/T$ , we find  $\hat{q} \approx 7 \pm 0.6 \text{ GeV}^2 \text{ fm}^{-1}$  at  $T = 500 \text{ MeV}$ . This number has been rescaled to the color factors appropriate to SU(3)<sup>6</sup>. Since  $E/T$  is fixed, this result corresponds to a jet energy of  $E = 48T = 24 \text{ GeV}$ . The quoted error arises from using different possible fits, including a logarithmic dependence on  $T$  or not, and from different choices for  $k^*$ . For a temperature of  $T = 400 \text{ MeV}$  and the corresponding thermal gluon

<sup>6</sup> We divide the results by the prefactors given in Eqs. (32) and (33), respectively, which correspond to  $N_c = 2$ , and multiply by the prefactors appropriate for  $N_c = 3$ .

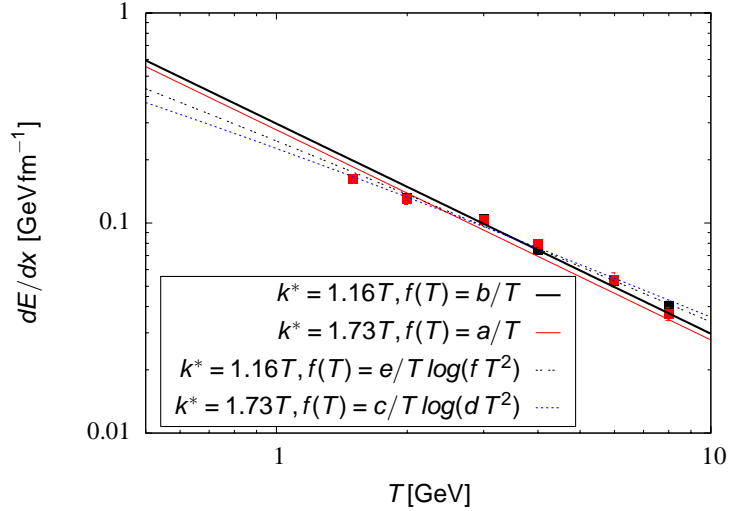


FIG. 8: Dependence of  $dE/dx$  on the temperature  $T$ .  $n = 5 \text{ fm}^{-3}$ ,  $g = 2$ ,  $k^* \approx 1.16T$  (black squares) and  $k^* \approx 1.73T$  (red/grey squares).  $a \dots f$  are fit parameters - the plot shows the best fits. Extrapolation to temperatures  $T \sim 500 \text{ MeV}$  leads to uncertainties of order 40 %.

density, we find  $\hat{q} \approx 3.6 \pm 0.3 \text{ GeV}^2 \text{ fm}^{-1}$  ( $E = 19.2 \text{ GeV}$ ). We emphasize that our simulations do not account for quarks and anti-quarks which would provide a sizeable contribution to the thermal density. Nevertheless, such values for  $\hat{q}$  are within the range extracted from RHIC data [59, 95, 96].

In Fig. 8 we present a possible extrapolation of  $dE/dx$  to temperatures around 500 MeV. We find  $dE/dx \approx 0.35 - 0.6 \text{ GeV fm}^{-3}$  at  $T = 500 \text{ MeV}$ , and for a jet energy of  $E = 48$ ,  $T = 24 \text{ GeV}$ . Adjusting for the different color factors for SU(3) and extrapolating to the thermal density of gluons we find  $dE/dx \approx 2.5 \pm 0.6 \text{ GeV fm}^{-1}$ . At  $T = 400 \text{ MeV}$ , the result is  $dE/dx \approx 1.6 \pm 0.4 \text{ GeV fm}^{-1}$  ( $E = 19.2 \text{ GeV}$ ).

In Figs. 9 and 10 we show how  $\hat{q}$  and  $dE/dx$  depend on the energy  $E$  of the jet. The behavior is logarithmic, in agreement with the perturbative expectation; compare to Eqs. (32) and (33), using  $Q^2 \sim ET$  (the explicit factor of  $E$  in the numerator cancels since  $\langle s \rangle = 6ET$ ). A fit of the numerical result to (32), using  $Q^2 \approx s$ , leads to  $C \approx 1.45$ , but is good only if an additional prefactor of  $\sim 0.63$  is allowed. This suggests that the perturbative result does not describe the numerical solution very well, which could perhaps be expected at  $g = 2$ . Repeating the analysis for  $dE/dx$  via Eq. (33), we find  $C' \approx 7.7$ ; again, a multiplicative factor needs to be included, this time it is  $\sim 0.036$ . Thus, for the jet energies considered

here, pQCD at LL appears to work less well for  $dE/dx$  than for  $\hat{q}$ .

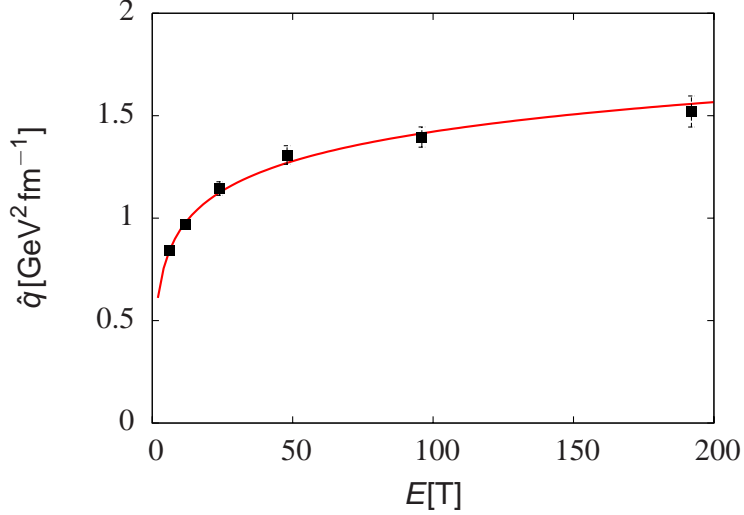


FIG. 9: Jet-energy dependence of  $\hat{q}$  for  $T = 4$  GeV and  $n = 5$  fm $^{-3}$ .  $k^* \approx 1.16 T$ . The line shows the fit to Eq. (32), with an overall multiplicative factor of 0.63.

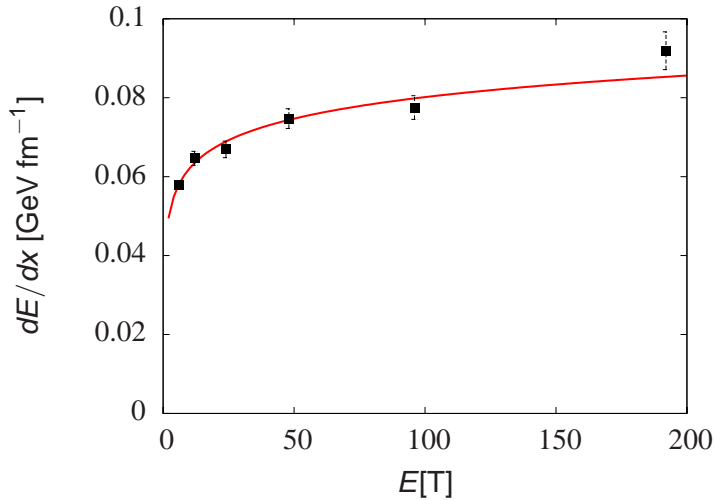


FIG. 10: Jet-energy dependence of  $dE/dx$  for  $T = 4$  GeV and  $n = 5$  fm $^{-3}$ .  $k^* \approx 1.16 T$ . The line shows the fit to Eq. (33), with an overall multiplicative factor of 0.036.

Finally, we show the full  $p_\perp^2$ -distribution of the high-momentum partons. We find that over time the initial  $\delta$ -function broadens to an exponential distribution with a power-law tail. Figs. 11 and 12 show the distribution of the high-momentum “jet” test particles after

$t \approx 2.8$  fm and  $t \approx 5.2$  fm, respectively, in a double-logarithmic plot versus  $p_\perp^2/t$ . We scale  $p_\perp^2$  by the inverse time so that the basic features of the distribution are nearly time independent. It turns out that an exponential fit describes the low- $p_\perp$  part somewhat better than a Gaussian, although we expect that a Gaussian shape will eventually emerge after many collisions. The power-law tail at large  $p_\perp$  behaves approximately as  $p_\perp^{-4}$ . This is expected for particles experiencing only few scatterings since in the high-energy limit the differential cross section  $d\sigma/dp_\perp^2 \sim p_\perp^{-4}$ , c.f. Eq. (20). This is the probability distribution for the momentum transfer in a single hard collision. In both figures we also indicate the value of  $\hat{q}$  to show that the power-law tail contributes significantly to its value. For the densities, temperatures and jet energies considered here it is clearly not a very good approximation to determine the transport coefficient  $\hat{q}$  from the Gaussian or exponential part of the distribution alone as this would underestimate  $\hat{q}$  substantially.

Note that transverse momenta on the order of the temperature ( $T = 4$  GeV), such as the separation scale  $k^* \approx 1.2T$ , correspond to  $p_\perp^2/t \approx 5.2 \text{ GeV}^2 \text{ fm}^{-1}$  in Fig. 11 and to  $p_\perp^2/t \approx 3 \text{ GeV}^2 \text{ fm}^{-1}$  in Fig. 12. Above this value for  $p_\perp^2/t$  the distribution is due almost entirely to hard collisions (we have checked that multiple soft collisions do not contribute much in that region).

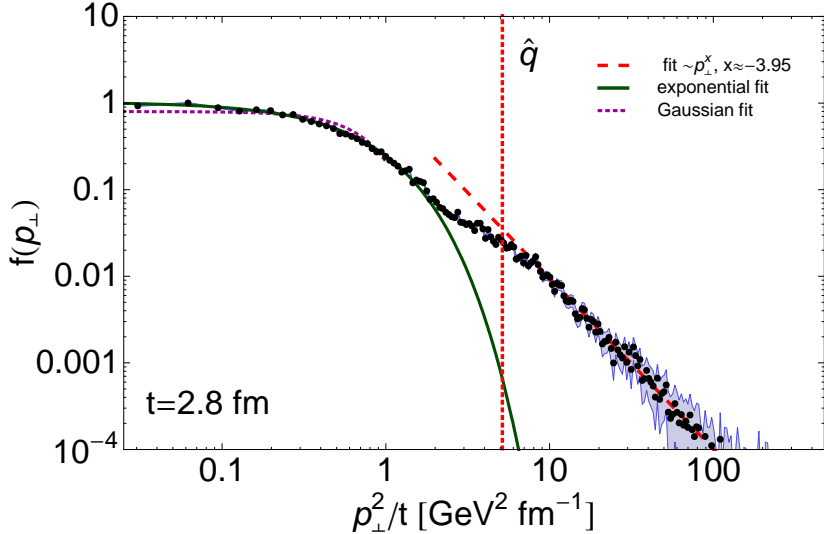


FIG. 11:  $p_\perp^2$ -distribution of the high-momentum “jet”-partons after  $t \approx 2.8$  fm for  $T = 4$  GeV and  $n_g = 20 \text{ fm}^{-3}$  ( $\hat{q} \approx 5.16 \text{ GeV}^2 \text{ fm}^{-1}$ ).

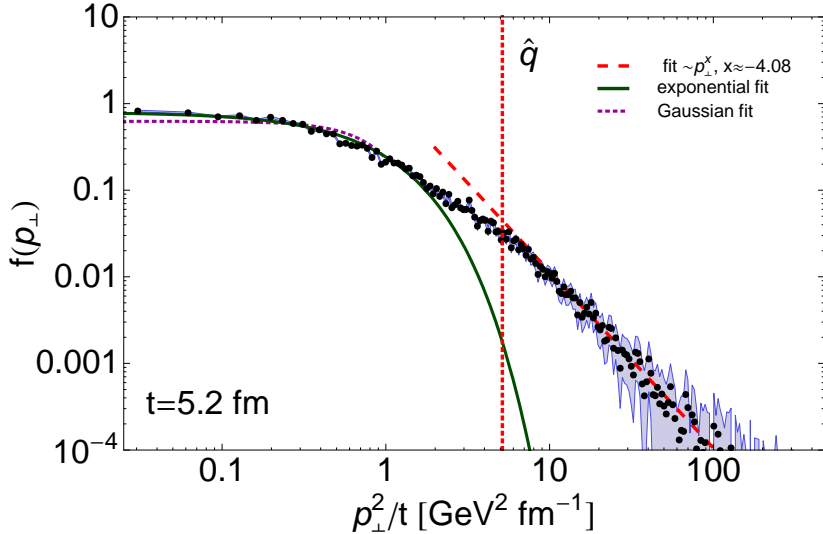


FIG. 12:  $p_{\perp}^2$ -distribution of the high-momentum “jet”-partons after  $t \approx 5.2$  fm for  $T = 4$  GeV and  $n_g = 20 \text{ fm}^{-3}$  ( $\hat{q} \approx 5.16 \text{ GeV}^2 \text{ fm}^{-1}$ ).

### B. Radiative energy loss

Whenever a (color-) charged particle receives a momentum kick (is accelerated) it emits radiation. As already mentioned before, soft classical radiation emerges in our approach via the color currents which enter the Yang-Mills equations as sources. However, in the present paper we do not consider *hard* inelastic collisions. Therefore, we do not expect the radiative energy loss to be lattice spacing (separation scale) independent.

Nevertheless, it is interesting to compare the overall magnitude of the combined radiative plus collisional energy losses to the purely collisional energy loss. In fact, we shall find that  $dE/dx|_{\text{rad}}$  is larger by at least an order of magnitude than  $dE/dx|_{\text{coll}}$  for all lattice spacings corresponding to reasonable separation scales  $k^* \sim T$ . For even smaller lattice spacing (larger  $k^*$ ) the radiative contribution would increase further but the classical approximation is expected to fail at large  $k$ .

The dependence of  $\hat{q}$  and of  $dE/dx$  on the lattice spacing  $a$  (for a *colored* jet) is shown in Fig. 13.  $dE/dx$  decreases rather rapidly with increasing  $a$  since the lattice spacing is inversely proportional to the wave vector of the highest available field mode. For the physically motivated prescription  $k^* \sim T$  (and  $k^* \sim 1/a$ ),  $a$  is larger for lower  $T$ . Hence, the lower  $T$ , the smaller the contribution from soft classical radiation to the total energy loss (e.g.,

$dE/dx|_{\text{total}} \approx 1 \text{ GeV fm}^{-1}$  for  $T = 2 \text{ GeV}$ ). Yet, it still exceeds the collisional energy loss at this density ( $n_g = 5 \text{ fm}^{-3}$ ) by an order of magnitude; compare to Fig. 4 from above. We therefore expect that when *hard* radiative processes are included, that for massless partons radiative energy loss will be large also for temperatures around  $400 - 500 \text{ MeV}$ . This agrees qualitatively with the comparison of collisional and radiative energy loss performed in ref. [97], and appears also to be in line with phenomenology from RHIC [98].

The transport coefficient  $\hat{q}$  also decreases somewhat on coarser lattices, but is not as sensitive to classical radiation as the energy loss  $dE/dx$ . The order of magnitude of  $\hat{q}$  is the same as for purely elastic processes (colorless jet). This is due to the fact that coherent bremsstrahlung is almost collinear such that the jet mainly loses longitudinal momentum. We conclude that  $\hat{q}$  is dominated by collisional broadening, at least as long as hard radiative processes are not considered.

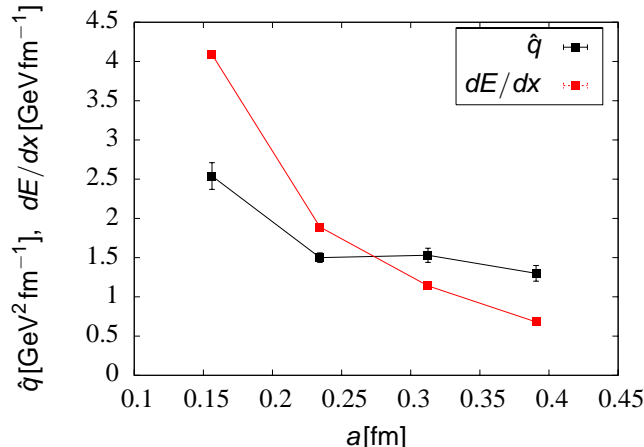


FIG. 13: Lattice spacing dependence of the combined radiative and collisional energy loss of a colored parton for  $T = 4 \text{ GeV}$ ,  $E = 48T$  and  $n_g = 5 \text{ fm}^{-3}$ . For  $T = 4 \text{ GeV}$ ,  $a = 0.156 \text{ fm}$  corresponds to  $k^* \approx 1.73T$  while  $a = 0.39 \text{ fm}$  corresponds to  $k^* \approx 0.69T$ .

## VIII. SUMMARY AND CONCLUSIONS

We have studied collisional and soft radiative energy loss as well as momentum broadening of high-momentum gluon jets in a hot and dense non-Abelian  $SU(2)$  plasma by solving the coupled system of Wong-Yang-Mills equations in real time on a lattice. We separate the

soft from the hard momentum exchange interactions by introducing a separation scale  $k^*$ . This separation scale is given by the inverse lattice spacing  $\sim 1/a$ , which determines the magnitude of the highest momentum field modes that can be represented on the lattice. We fix its physical value to be on the order of the temperature. Momentum exchanges below that scale are mediated by the classical fields, those above the separation scale by direct elastic collisions between the particles. The latter were implemented through the pQCD collision term and the stochastic method for determining scattering probabilities.

In our approach, collisional energy loss can be separated from the radiative part by simulating effectively colorless jets (at the scale set by the lattice spacing). We were able to obtain lattice-spacing and hence separation-scale independent results for  $\hat{q}$  and  $dE/dx$  in a static plasma. The dependence on temperature and density, as well as on the jet energy was found to follow qualitatively expectations from pQCD. We then extrapolated our simulation results to thermal densities and to realistic temperatures of about 500 MeV, which could not be simulated directly due to numerical reasons. For a thermal gluon plasma (no quarks and anti-quarks) at  $T = 400$  MeV, and with color factors adjusted to the SU(3) gauge group, we estimate  $\hat{q} \approx 3.6 \pm 0.3$  GeV $^2$ fm $^{-1}$  and  $dE/dx \approx 1.6 \pm 0.4$  GeVfm $^{-1}$ , for a jet energy of 19.2 GeV. The errors are mainly due to the required extrapolation. At finite time (on the order of the transverse dimension of the collision zone), the  $p_\perp^2$ -distribution of the high-momentum partons is found to be well approximated by an exponential at low  $p_\perp$  and to exhibit a power-law tail  $\sim p_\perp^{-4}$  at high  $p_\perp$ . The first moment of the distribution, i.e. the transport coefficient  $\hat{q}$ , receives a large contribution from the power-law tail.

Jets with non-zero effective color charge can also emit “soft” bremsstrahlung with  $k$  up to  $k^* \sim T$ . We find that at extremely high temperature,  $T \gtrsim 1 - 2$  GeV, such classical radiation increases  $dE/dx$  by an order of magnitude as compared to that due to elastic collisions. On the other hand, transverse momentum diffusion ( $\hat{q}$ ) is not modified by much. Such radiation above the thermal wavelength may thermalize rather quickly and heat the medium. However, so far we were unable to perform reliable extrapolations of the radiative energy loss to more realistic temperatures of  $T \sim 500$  MeV and so the relative magnitude of collisional versus radiative energy loss at such temperatures is not entirely clear. While classical radiation into the window  $k < T$  is bound to decrease (as we have shown), this should be compensated at least in part by hard pQCD radiation.

In the future, the present approach should be extended to include hard particle splittings

and recombination in order to fully address medium-induced  $p_\perp$  broadening and energy loss of a colored high momentum parton at leading order [99, 100, 101].

### Acknowledgments

We thank Oliver Fochler, Charles Gale, Berndt Müller, and Zhe Xu for helpful discussions and comments. The simulations were performed at the Center for Scientific Computing (CSC) of Goethe University, Frankfurt am Main. M.S. and B.S. were in part supported by DFG Grant GR 1536/6-1. B.S. gratefully acknowledges a Richard H. Tomlinson Fellowship awarded by McGill University as well as support from the Natural Sciences and Engineering Research Council of Canada. Y.N. is supported by Japan MEXT grant No. 20540276. M.S. and Y.N. acknowledge support from the Yukawa Institute for Theoretical Physics during the “Entropy Production Before QGP” workshop.

---

- [1] M. Gyulassy and X.-N. Wang, Nucl. Phys. **B420**, 583 (1994), nucl-th/9306003.
- [2] C. Adler et al. (STAR), Phys. Rev. Lett. **89**, 202301 (2002), nucl-ex/0206011.
- [3] K. Adcox et al. (PHENIX), Phys. Rev. Lett. **88**, 022301 (2002), nucl-ex/0109003.
- [4] P. Jacobs, Eur. Phys. J. **C43**, 467 (2005), nucl-ex/0503022.
- [5] S. S. Adler et al. (PHENIX), Phys. Rev. Lett. **94**, 232301 (2005), nucl-ex/0503003.
- [6] J. Adams et al. (STAR), Phys. Rev. Lett. **91**, 172302 (2003), nucl-ex/0305015.
- [7] H. Busching et al. (PHENIX), Eur. Phys. J. **C43**, 303 (2005).
- [8] R. Baier, Y. L. Dokshitzer, A. H. Mueller, S. Peigne, and D. Schiff, Nucl. Phys. **B484**, 265 (1997), hep-ph/9608322.
- [9] R. Baier, Y. L. Dokshitzer, A. H. Mueller, and D. Schiff, Phys. Rev. **C58**, 1706 (1998), hep-ph/9803473.
- [10] B. G. Zakharov, JETP Lett. **63**, 952 (1996), hep-ph/9607440.
- [11] B. G. Zakharov, Pisma Zh. Eksp. Teor. Fiz. **64**, 737 (1996), hep-ph/9612431.
- [12] B. G. Zakharov, JETP Lett. **65**, 615 (1997), hep-ph/9704255.
- [13] B. G. Zakharov, Phys. Atom. Nucl. **61**, 838 (1998), hep-ph/9807540.
- [14] B. G. Zakharov, JETP Lett. **70**, 176 (1999), hep-ph/9906536.

- [15] B. G. Zakharov, JETP Lett. **73**, 49 (2001), hep-ph/0012360.
- [16] M. Gyulassy, P. Levai, and I. Vitev, Nucl. Phys. **B594**, 371 (2001), nucl-th/0006010.
- [17] S. Jeon and G. D. Moore, Phys. Rev. **C71**, 034901 (2005), hep-ph/0309332.
- [18] C. A. Salgado and U. A. Wiedemann, Phys. Rev. **D68**, 014008 (2003), hep-ph/0302184.
- [19] S. Wicks, W. Horowitz, M. Djordjevic, and M. Gyulassy, Nucl. Phys. **A784**, 426 (2007), nucl-th/0512076.
- [20] O. Fochler, Z. Xu, and C. Greiner (2008), arXiv:0806.1169.
- [21] K. Miki (PHENIX), Talk given at “20th International Conference on Nucleus Nucleus Collisions” (Quark Matter 2008), February 4–10, 2008, Jaipur, India - proceedings to be published in J. Phys. G. (2008).
- [22] C. Adler et al. (STAR), Phys. Rev. Lett. **90**, 082302 (2003), nucl-ex/0210033.
- [23] S. S. Adler et al. (PHENIX), Phys. Rev. Lett. **97**, 052301 (2006), nucl-ex/0507004.
- [24] H. G. Baumgardt et al., Z. Phys. **A273**, 359 (1975).
- [25] H. Stoecker, B. Betz, and P. Rau, PoS **CPOD2006**, 029 (2006), nucl-th/0703054.
- [26] B. Baeuchle, L. P. Csernai, and H. Stoecker (2007), arXiv:0710.1476.
- [27] J. Casalderrey-Solana, E. V. Shuryak, and D. Teaney, J. Phys. Conf. Ser. **27**, 22 (2005), hep-ph/0411315.
- [28] B. Betz, M. Gyulassy, D. H. Rischke, H. Stocker, and G. Torrieri (2008), arXiv:0804.4408.
- [29] B. Betz, M. Gyulassy, J. Noronha, and G. Torrieri (2008), arXiv:0807.4526.
- [30] J. Putschke, J. Phys. **G34**, S679 (2007), nucl-ex/0701074.
- [31] J. Adams et al. (STAR), Phys. Rev. **C73**, 064907 (2006), nucl-ex/0411003.
- [32] C. Nattrass (2008), arXiv:0809.5261.
- [33] J. Adams et al. (STAR), Phys. Rev. Lett. **95**, 152301 (2005), nucl-ex/0501016.
- [34] F. Wang (STAR), J. Phys. **G30**, S1299 (2004), nucl-ex/0404010.
- [35] N. Armesto, C. A. Salgado, and U. A. Wiedemann, Phys. Rev. Lett. **93**, 242301 (2004), hep-ph/0405301.
- [36] C. B. Chiu and R. C. Hwa, Phys. Rev. **C72**, 034903 (2005), nucl-th/0505014.
- [37] P. Romatschke and M. Strickland, Phys. Rev. **D69**, 065005 (2004), hep-ph/0309093.
- [38] P. Romatschke and M. Strickland, Phys. Rev. **D71**, 125008 (2005), hep-ph/0408275.
- [39] P. Romatschke, Phys. Rev. **C75**, 014901 (2007), hep-ph/0607327.
- [40] A. Majumder, B. Muller, and S. A. Bass, Phys. Rev. Lett. **99**, 042301 (2007), hep-

ph/0611135.

- [41] A. Dumitru, Y. Nara, B. Schenke, and M. Strickland, Phys. Rev. **C78**, 024909 (2008), arXiv:0710.1223.
- [42] B. Schenke, A. Dumitru, Y. Nara, and M. Strickland (2008), arXiv:0804.4557.
- [43] C.-Y. Wong (2007), arXiv:0712.3282.
- [44] R. C. Hwa and C. B. Yang (2008), arXiv:0801.2183.
- [45] A. Dumitru, F. Gelis, L. McLerran, and R. Venugopalan (2008), arXiv:0804.3858.
- [46] C.-Y. Wong (2008), arXiv:0806.2154.
- [47] S. K. Wong, Nuovo Cim. **A65S10**, 689 (1970).
- [48] C. R. Hu and B. Muller, Phys. Lett. **B409**, 377 (1997), hep-ph/9611292.
- [49] A. Krasnitz and R. Venugopalan, Nucl. Phys. **B557**, 237 (1999), hep-ph/9809433.
- [50] A. Krasnitz and R. Venugopalan, Phys. Rev. Lett. **84**, 4309 (2000), hep-ph/9909203.
- [51] A. Krasnitz, Y. Nara, and R. Venugopalan, Phys. Rev. Lett. **87**, 192302 (2001), hep-ph/0108092.
- [52] A. Krasnitz, Y. Nara, and R. Venugopalan, Nucl. Phys. **A717**, 268 (2003), hep-ph/0209269.
- [53] A. Krasnitz, Y. Nara, and R. Venugopalan, Nucl. Phys. **A727**, 427 (2003), hep-ph/0305112.
- [54] A. Krasnitz, Y. Nara, and R. Venugopalan, Phys. Lett. **B554**, 21 (2003), hep-ph/0204361.
- [55] A. Dumitru and Y. Nara, Phys. Lett. **B621**, 89 (2005), hep-ph/0503121.
- [56] A. Dumitru, Y. Nara, and M. Strickland, Phys. Rev. **D75**, 025016 (2007), hep-ph/0604149.
- [57] L. D. McLerran and R. Venugopalan, Phys. Rev. **D49**, 2233 (1994), hep-ph/9309289.
- [58] A. H. Mueller and D. T. Son, Phys. Lett. **B582**, 279 (2004), hep-ph/0212198.
- [59] S. A. Bass et al. (2008), arXiv:0808.0908.
- [60] U. W. Heinz, Phys. Rev. Lett. **51**, 351 (1983).
- [61] U. W. Heinz, Ann. Phys. **161**, 48 (1985).
- [62] U. W. Heinz, Ann. Phys. **168**, 148 (1986).
- [63] H.-T. Elze and U. W. Heinz, Phys. Rept. **183**, 81 (1989).
- [64] P. F. Kelly, Q. Liu, C. Lucchesi, and C. Manuel, Phys. Rev. Lett. **72**, 3461 (1994), hep-ph/9403403.
- [65] P. F. Kelly, Q. Liu, C. Lucchesi, and C. Manuel, Phys. Rev. **D50**, 4209 (1994), hep-ph/9406285.
- [66] J.-P. Blaizot and E. Iancu, Nucl. Phys. **B557**, 183 (1999), hep-ph/9903389.

- [67] M. Laine and C. Manuel, Phys. Rev. **D65**, 077902 (2002), hep-ph/0111113.
- [68] G. F. Bertsch and S. Das Gupta, Phys. Rept. **160**, 189 (1988).
- [69] D. F. Litim and C. Manuel, Nucl. Phys. **B562**, 237 (1999), hep-ph/9906210.
- [70] D. F. Litim and C. Manuel, Phys. Rev. Lett. **82**, 4981 (1999), hep-ph/9902430.
- [71] G. D. Moore, C.-r. Hu, and B. Muller, Phys. Rev. **D58**, 045001 (1998), hep-ph/9710436.
- [72] J. Ambjorn, T. Askgaard, H. Porter, and M. E. Shaposhnikov, Nucl. Phys. **B353**, 346 (1991).
- [73] J. B. Kogut and L. Susskind, Phys. Rev. **D11**, 395 (1975).
- [74] T. Kodama, S. B. Duarte, K. C. Chung, R. Donangelo, and R. A. M. S. Nazareth, Phys. Rev. C **29**, 2146 (1984).
- [75] K. Geiger and B. Muller, Nucl. Phys. **B369**, 600 (1992).
- [76] G. Kortemeyer, W. Bauer, K. Haglin, J. Murray, and S. Pratt, Phys. Rev. **C52**, 2714 (1995), nucl-th/9509013.
- [77] B. Zhang, M. Gyulassy, and Y. Pang, Phys. Rev. **C58**, 1175 (1998), nucl-th/9801037.
- [78] S. Cheng et al., Phys. Rev. **C65**, 024901 (2002), nucl-th/0107001.
- [79] G. Welke, R. Malfliet, C. Grégoire, M. Prakash, and E. Suraud, Phys. Rev. C **40**, 2611 (1989).
- [80] D. Molnar and M. Gyulassy, Nucl. Phys. **A697**, 495 (2002), nucl-th/0104073.
- [81] X.-M. Xu, Y. Sun, A.-Q. Chen, and L. Zheng, Nucl. Phys. **A744**, 347 (2004).
- [82] Z. Xu and C. Greiner, Phys. Rev. **C71**, 064901 (2005), hep-ph/0406278.
- [83] Z. Xu and C. Greiner, Phys. Rev. **C76**, 024911 (2007), hep-ph/0703233.
- [84] S. Mrowczynski, Phys. Lett. **B393**, 26 (1997), hep-ph/9606442.
- [85] P. Romatschke and M. Strickland, Phys. Rev. **D68**, 036004 (2003), hep-ph/0304092.
- [86] S. Mrowczynski, A. Rebhan, and M. Strickland, Phys. Rev. **D70**, 025004 (2004), hep-ph/0403256.
- [87] P. Romatschke and M. Strickland, Phys. Rev. **D70**, 116006 (2004), hep-ph/0406188.
- [88] P. Danielewicz and G. F. Bertsch, Nucl. Phys. **A533**, 712 (1991).
- [89] A. Lang, H. Babovsky, W. Cassing, U. Mosel, H. Reusch, and K. Weber, J. Comp. Phys. **106**, 391 (1993).
- [90] S. de Groot, W. van Leeuwen, and C. van Weert, *Relativistic Kinetic Theory: Principles and Applications* (North Holland, Amsterdam, 1980).
- [91] B. L. Combridge, J. Kripfganz, and J. Ranft, Phys. Lett. **B70**, 234 (1977).

- [92] J. F. Owens, E. Reya, and M. Gluck, Phys. Rev. **D18**, 1501 (1978).
- [93] Z. Bern, A. De Freitas, and L. J. Dixon, JHEP **03**, 018 (2002), hep-ph/0201161.
- [94] A. Dumitru and M. Gyulassy, Phys. Lett. **B494**, 215 (2000), hep-ph/0006257.
- [95] A. Majumder, J. Phys. **G34**, S377 (2007), nucl-th/0702066.
- [96] R. Baier and D. Schiff, JHEP **09**, 059 (2006), hep-ph/0605183.
- [97] G.-Y. Qin et al., Phys. Rev. Lett. **100**, 072301 (2008), arXiv:0710.0605.
- [98] T. Renk, Phys. Rev. **C76**, 064905 (2007), arXiv:0708.4319.
- [99] P. Arnold, G. D. Moore, and L. G. Yaffe, JHEP **11**, 057 (2001), hep-ph/0109064.
- [100] P. Arnold, G. D. Moore, and L. G. Yaffe, JHEP **12**, 009 (2001), hep-ph/0111107.
- [101] P. Arnold, G. D. Moore, and L. G. Yaffe, JHEP **06**, 030 (2002), hep-ph/0204343.